Branko Damjanac, Peter A. Cundall and Terje Brandshaug

Itasca Presentations at the Menlo Park Workshop, August 23-24, 2004

BACKGROUND

This memorandum presents summaries of presentations by Drs. Peter Cundall and Branko Damjanac at the Workshop on Extreme Ground Motions at Yucca Mountain, Menlo Park, California, August 23-24, 2004. The two presentations are summarized in Sections 2 and 3, respectively.

1.0 FULLY NON-LINEAR MODELING OF DYNAMIC TRANSMISSION IN ROCK

The currently accepted methodology for calculating the transmission of seismic motion from source to site is the equivalent linear method (ELM), which is an approximate method, described as follows.

> A ***series*** of linear analyses is performed, with constant (but different) values of damping ratio and shear modulus at various locations in the model. The observed maximum cyclic shear strain in each element is used to determine values for damping and modulus for the next analysis using laboratory-derived curves — "degradation curves." The process is repeated several times, until there is no further change in properties. At this point, it is said that "strain-compatible" values of damping and modulus have been found.

The method has been found to give reasonable results for ground motions commonly considered in Civil Engineering (e.g., less than 1 g), but it is unknown if the method is good enough for very high amplitude motions. To be rigorous, we should compare the results of ELM analyses with full, non-linear simulations (FNL), for high-amplitude wave propagation. Itasca recently received an S&T contract to study this topic in detail; we simply present here some background and preliminary results (because the work has only just started). A comparison of the treatment of effects and mechanisms of the two methods is shown in Table 1.

Table 1 Comparison between equivalent-linear and fully non-linear methods

Equivalent-linear method (ELM)	Fully non-linear method (FNL)
Properties are constant over time — e.g., overdamped in quiet periods; underdamped for periods of strong-motion.	Damping and modulus appropriate to amplitude at all times.
Interference & mixing between frequencies absent.	Interference & mixing occur naturally.
Irreversible strains not modeled directly.	Irreversible strains accumulated.
Stress and strain increments coaxial in elastic law.	Proper flow rule: independent strain increment.
Shape of hysteresis law (an ellipse) is built in.	Any form of hysteretic law may be used.
No coupling between P and S wave components.	Full, non-linear coupling between P & S (e.g., change in shear strength due to P wave).

1.1 Direct Comparison Between ELM & FNL for Modest Strains

The equivalent-linear code SHAKE was compared with *FLAC* (a continuum FD code), using the example found on the SHAKE web site (a series of soil layers, of increasing modulus with depth). Details of the comparison are found in the *FLAC* user's manual (Itasca, 2004). The Loma Prieta horizontal acceleration record was used, scaled to various maximum acceleration levels. *FLAC* used a fully non-linear law (with memory of reversal points): an example of the stress/strain path at the middle of the soil profile is reproduced in Figure 1. The comparison of surface acceleration amplification-factor (between SHAKE and *FLAC*) is shown in Figure 2, for base excitation up to 1g. There is reasonable agreement between the ELM and FNL method for this case.

1.2 Simple Example of the Effect of Simultaneous P-Wave and S-Wave Propagation

The ELM does not include the coupling effects of shear and compressional strains, which may be important — for example, if a momentary reduction of normal stress leads to increased shear yielding. Using the same seismic history as the previous example, a 1 Km-high column of Mohr-Coulomb, perfectly plastic material is used. There is a Gaussian standard deviation of friction angle = 7.5^{o}, with a mean of 30^{o}. This produces a quasi-continuous yield function for the ensemble. P-wave input also is applied, of varying magnitude. This time history is the *time-reversed* S-wave history (to give the same spectrum, but almost zero time correlation). 0 shows the effect (on the horizontal surface acceleration) both with and without simultaneous P-wave excitation.

The effect of a simultaneous P-wave excitation is to increase the mean horizontal motion during the quiet period and decrease it during the strong-motion period, but the mean acceleration and mean energy transmission are almost unchanged.

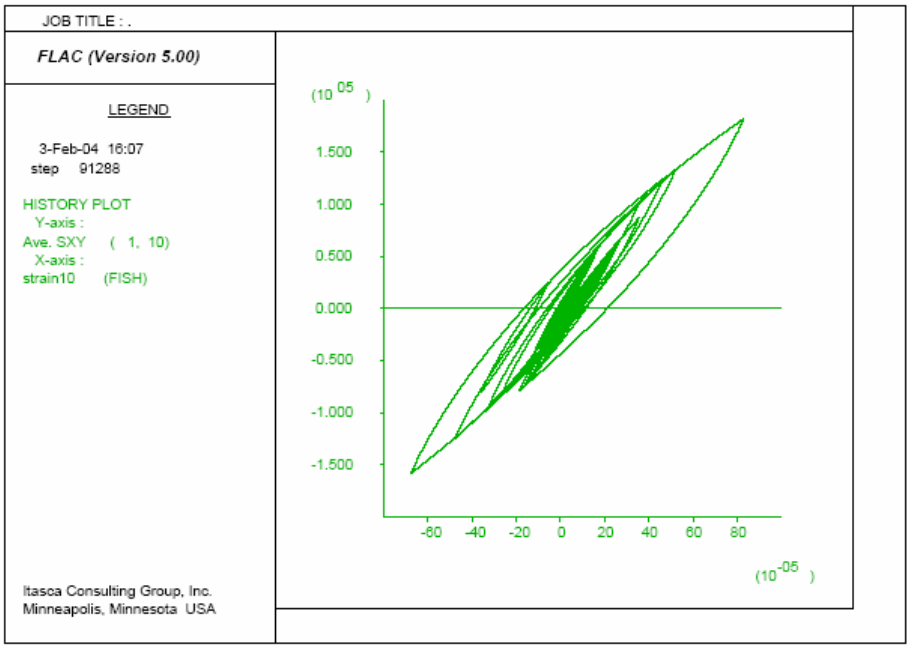

Figure 1 Shear stress/strain path in the middle of the soil profile

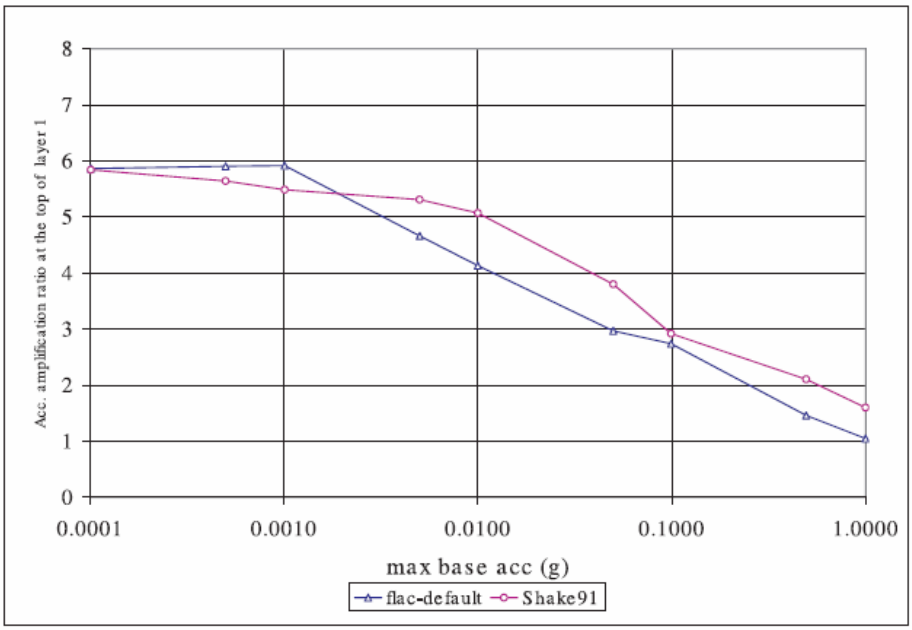

Figure 2 Amplification factor (for surface acceleration) versus base acceleration

Surface horizontal acceleration vs time: Left, zero P-wave amplitude; Right, equal P- and S-wave input (Max input horizontal acceleration = 4.5 g)

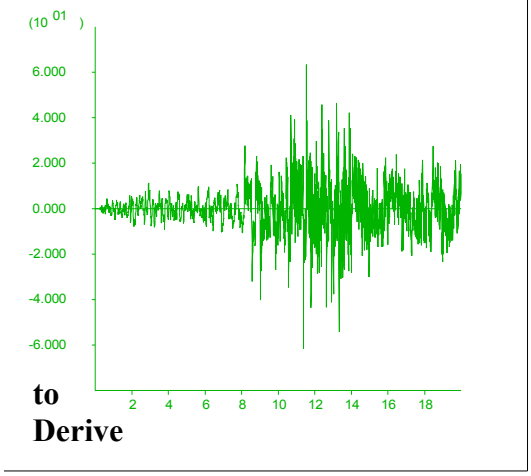

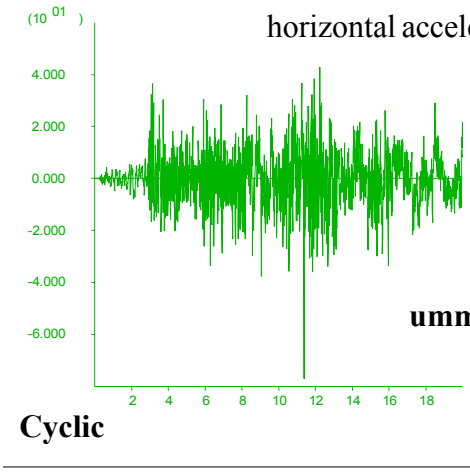

to Derive Cyclic ummary of Study Response of Large-Scale Rock Units at Yucca Mountain (Degradation Curves)

It is impossible to determine, experimentally, the appropriate cyclic degradation response for the major geological units. First, these units are in the order of 10 m to 100 m thick, and, second, the large-strain response is needed for strong-motion propagation calculations. We have constructed numerical models of the jointed rock units, based on all available geological and laboratory data (e.g., fracture maps, joint shear tests and intact rock tests). These models are exercised by cyclic loading, and degradation curves are derived from steady-state hysteresis loops. Figure 3 shows a typical joint structure for the Prow Pass unit (modeled with code *UDEC*) and the resulting hysteresis loops. The lower plots show stress tensors and open joints at the extreme points on the steady-state hysteresis loop: it is notable that shear strain alone causes tensile separation. Although the tests were performed on a "sample" with sinusoidal excitation, the same methodology could be applied to the propagation of synthetic seismic histories through the complete transmission path at the site.

1.4 Dynamic Wave Propagation through Jointed Rock at the Yucca Mountain Site

Itasca has performed many simulations of the response of the rock around the repository to supplied seismic motion. Several cases were repeated, for the 10^{-6} probability level, but with the repository opening omitted — i.e., the new simulations represent wave propagation through non-linear rock. Space precludes the inclusion of all the results, but, as an example, Figure 5 shows the final rock state after the passage of the S-wave alone; the magenta lines represent fractures that have yielded or opened. Figure 4 illustrates the stress paths followed for three cases. As noted previously, tensile cracking occurs during cyclic shear loading only. (The addition of P-wave loading increases the area of cracking).

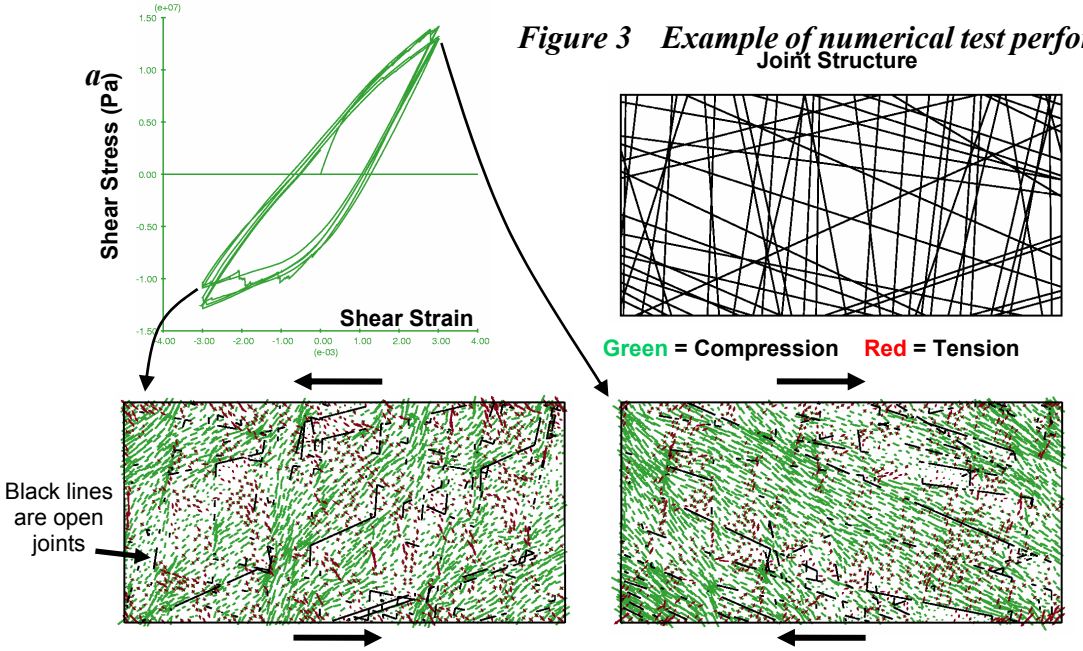

Figure 3 Example of numerical test performed on jointed rock unit (Prow Pass) to obtain hysteresis loops and, hence, degradation curves for the unit

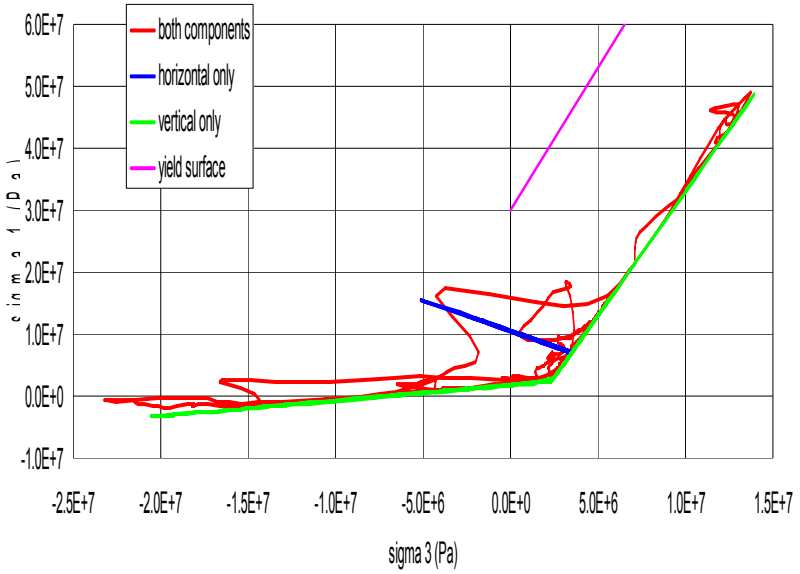

Figure 4 Stress paths followed during the seismic histories used in dynamic wave propagation through site rock (major principal stress vs minor principal stress)

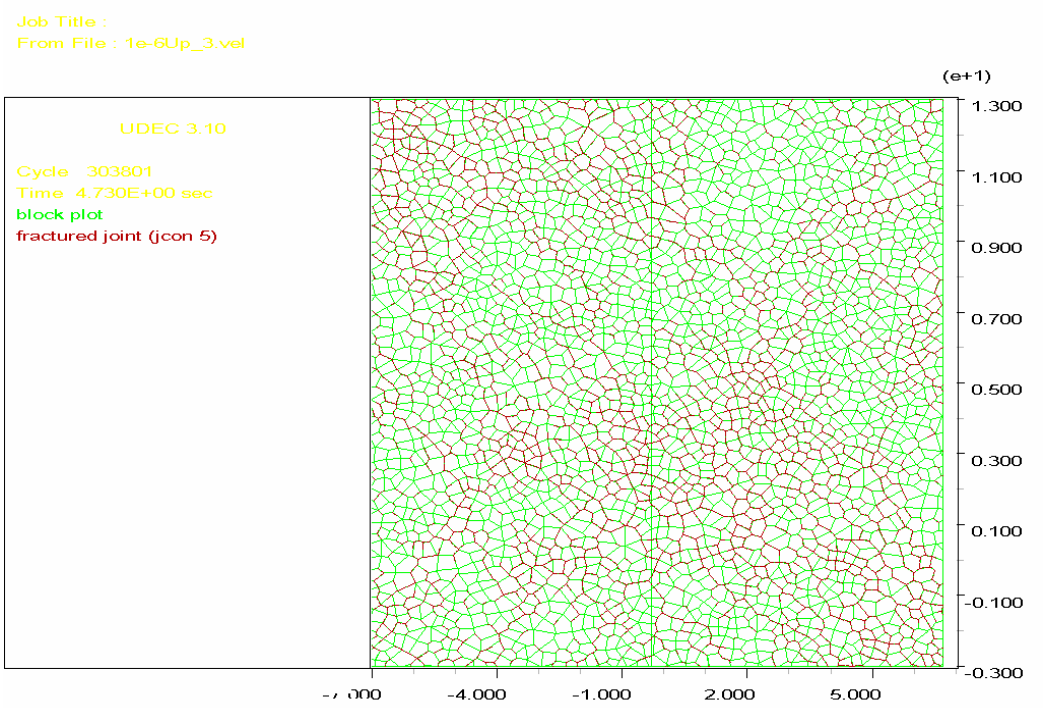

Figure 5 Final rock state after passage of seismic P-wave (10^{-6} probability level): magenta lines indicate yielded or open fractures

1.5 Conclusions

We have demonstrated that the means exists to perform fully non-linear simulations of wave propagation through — and below — the site. Some simple examples have been presented to indication the nature of such simulations, but a systematic study should be made of nonlinear wave transmission from source to site in order to validate (or not) the currently used equivalent-linear method (ELM), which is being applied well outside of its normal range of strain level. Preliminary results (for a few simple cases) indicate that the ELM is surprisingly good, even at high levels of motion.

2.0 ROCK MECHANICS ANALYSIS OF ABSENCE OF SEISMIC DAMAGE IN LITHOPHYSAL UNITS

The only credible way to provide limits to the maximum peak ground velocity (PGV) of the synthetic time histories used as input to seismic analyses for the Yucca Mountain Project is to estimate the maximum PGV that could have been experienced at the site in the geological past. To make this estimate, at least two pieces of evidence are necessary:

(1) observations of strain-induced fractures around lithophysae (or lack of such fractures); and

(2) data on the mean strain necessary to initiate fracturing around lithophysae and slip on joints.

Evidence in the first category is available from observations in the Exploratory Study Facility (ESF) and Enhanced Characterization of Repository Block (ECRB) Cross-Drift that indicate that the major-

ity of the fractures in the lithophysal and nonlithophysal units are induced thermally. To supply evidence in the second category, and to determine the upper bound to the seismically induced strain experienced by the Topopah Spring tuff since it has cooled off, the shear strain increments required to cause fracturing of the lithophysal rock mass were calculated based on results of the laboratory experiments (for units in which the proper test results are available) and results of the PFC and UDEC numerical micro-mechanical models.

The numerical results of PFC and UDEC, based on and calibrated to results of laboratory tests, were used to extrapolate experimental results to wider ranges of lithophysal porosity and different loading conditions that could not be tested in the laboratory (e.g., laboratory tests were conducted for unconfined conditions only). The numerical models also were used to establish the relation between different states of damage evolution and strain. Only the strain at peak stress could be determined from the laboratory results.

2.1 Damage States in Lithophysal Tuff

First, a decision must be made about the damage state (limiting state) at which fracturing would be observable in the field. Clearly, the state at which the first micro-cracks appear would be an underestimate (even though it is recorded in the numerical test), because a few unconnected cracks would be unnoticed in both the field and in the laboratory. Three states were considered: (a) the state at which the volumetric strain rate reverses (from compaction to expansion); (b) the onset of systematic fracturing (OSF); and (c) the state at which the peak stress occurs (i.e., the strength of the sample).

Figure 6 illustrates typical fracturing (at the point when the sample is strained beyond the peak stress) that occurs in a PFC sample in which lithophysal holes are represented as circular voids. There usually is considerable damage (e.g., blue fractures in Figure 6) at the peak stress point. Note that most of the stress-induced fractures connect lithophysae, so it should be possible to distinguish them — in underground observations — from other types of fractures, such as cooling fractures. The state at the peak stress is certainly an upper bound to a strain for which the fractures connecting lithophysae would be visible in the ESF and the ECRB cross-drift. The state at volumetric strain reversal is associated with significant damage, as the sample ceases to behave as an elastic continuum. (Structural change, due to cracks, is the reason for volumetric expansion.) The strain at volumetric strain reversal is less than the strain at the peak stress. The strain at the peak stress can be determined from the data collected during the laboratory test. Unfortunately, the collected information during the tests is insufficient to determine strain at the volumetric strain reversal or any other damage state (except at the peak stress).

One of the advantages of numerical tests on synthetic models of rock is the ability to monitor evolution of damage much more precisely and at finer detail (at practically no additional cost) than is possible in the laboratory. Numerical models allow determination of OSF by direct monitoring of formation and propagation of macro cracks by coalescence of micro cracks. An algorithm for monitoring the evolution of microcracks has been developed and used in PFC simulations of uniaxial compressive tests on the lithophysal rock mass. These results justify use of the states at peak stress and volumetric strain reversal as conservative estimates of the damage state at which fracturing would be observable in the field.

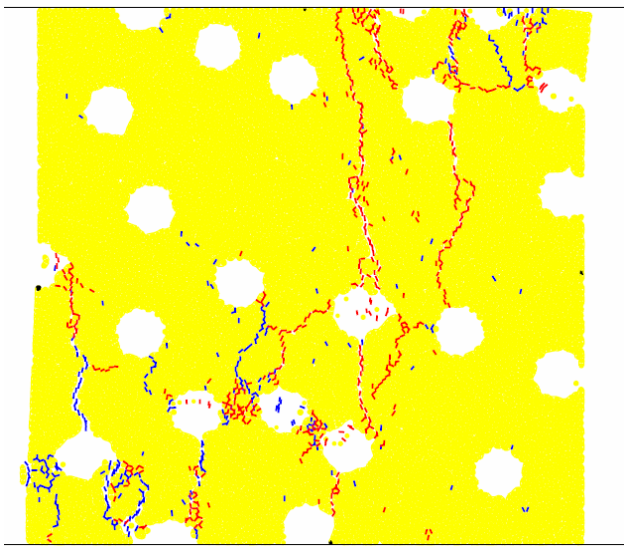

Figure 6 Fractures developed in lithophysal sample (blue = pre-peak, red = post-peak)

2.2 Methodology for Calculation of Strain Increment

The axial strain to a selected damage state (e.g., failure or state at peak stress, or OSF) cannot be used as the stain increment required to cause fracturing of lithophysal rock, because the axial strain measured in the laboratory corresponds to a certain uniaxial stress (and corresponding strain) path from the initial, unstressed state to the damage state. The rock mass exposed in the Yucca Mountain ESF and ECRB Cross-Drift is under an in-situ state of stress (strain) with a significant deviatoric component. (The horizontal principal stresses are between 30% and 60% of the vertical principal stress.) The shear-strain increment that causes stress change from an arbitrary initial stress state to a state on a surface (or line) in stress space that defines a limiting stress state (corresponding to a selected damage state) is calculated. The stress path from the initial stress state to the limiting damage state during a strong seismic ground motion can be arbitrary. In this analysis, the shear strain increment is calculated for the stress path in which the mean stress does not change (see Figure 7).

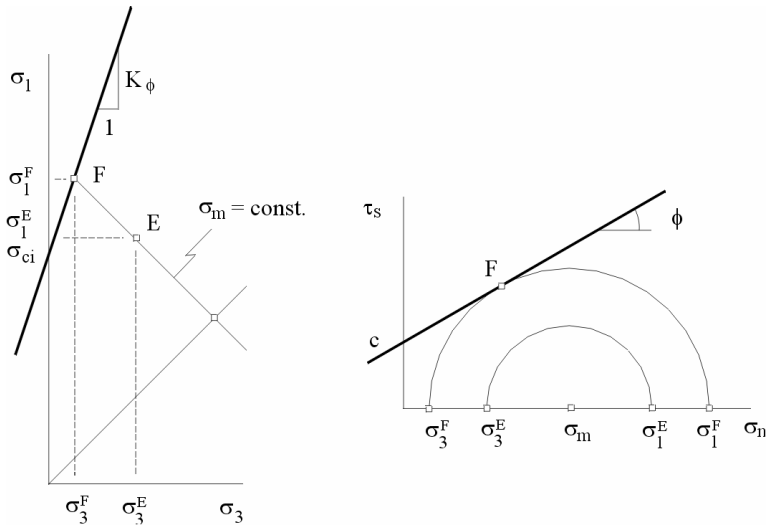

Figure 7 Rock Mechanics Analysis of Absence of Seismic Damage in Lithophysal Units

2.3 Shear Strain Limits Estimated from Laboratory Results

A large number of experiments was conducted on the samples from Topopah Spring tuff, both lithophysal and nonlithophysal. Testing of lithophysal tuff is particularly challenging because of lithophysal porosity, which makes preparation of the test samples very difficult. As expected, the mechanical properties of the lithophysal tuff exhibit strong size dependency. Therefore, the results obtained from the tests on the largest samples, 288-mm diameter cores taken from the ESF and ECRB Cross-Drift, are considered to be the best representation of the mechanical behavior of the lithophysal tuff. The shear strain increments were calculated for all laboratory results obtained on 288-mm diameter samples taken from the ESF and ECRB Cross-Drift. The experimental results were obtained for unconfined conditions only. A friction angle of 30º was assumed in the calculation. This assumption is conservative, because the friction angle of the lithophysal rock is probably in the range of 40º, which results in smaller strain increment. The results for the 288-mm diameter samples, divided into two categories based on height-to-diameter ratio ($H/D > 1.5$ and $H/D \leq 1.5$), are shown in Figure 8 as a function of lithophysal porosity.

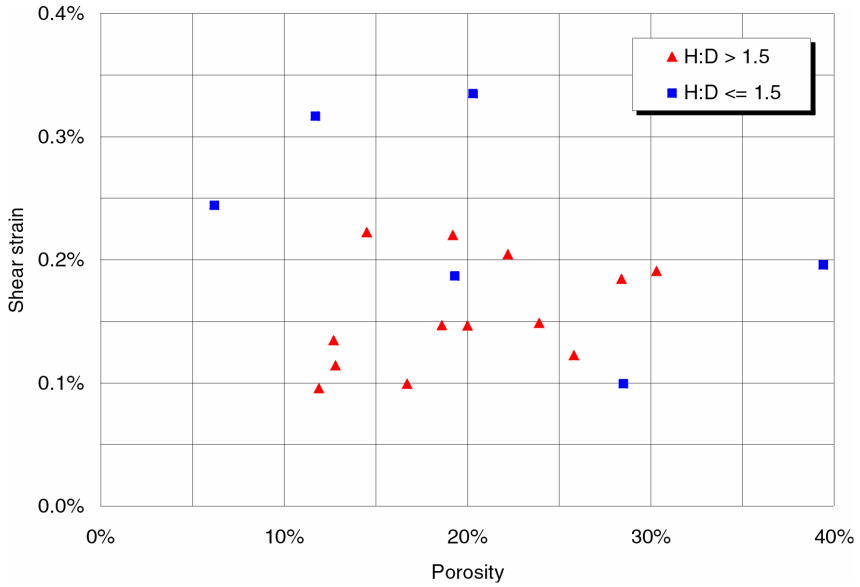

Figure 8 Calculated shear strain limit for 288-inch diameter samples

2.4 Shear Strain Limits Estimated from Numerical Results

The numerical models of the lithophysal rock mass first were calibrated to the results of the laboratory tests on samples with a certain lithophysal porosity. Subsequently, the effects of changing lithophysal porosity and shape of lithophysae were investigated. Thus, in the numerical analysis, it is assumed that lithophysal porosity and lithophysae shape are the only parameters affecting mechanical behavior of the lithophysal rock mass. This probably is the main reason the numerical results show less scatter than that observed in the laboratory tests.

The shear strain increments are calculated for the state of volumetric strain reversal and the state at peak stress. The PFC samples were tested for unconfined conditions only. A friction angle of 30º was assumed in calculating the shear strain increment based on PFC results. The UDEC samples were tested for both unconfined and confined conditions. The friction angle determined from the UDEC results was used in the calculating the shear strain increment based on UDEC results. The results for three types of 2D simulation are superimposed on each graph shown in Figure 9: (a) circular voids, modeled by PFC; (b) irregular (stencil) voids, modeled by PFC; and (c) circular voids, modeled by UDEC. The shear strain increments are calculated for two different levels of confining stress (250 m and 400 m of overburden) and two different assumptions about the damage state at which fracturing would be visible (reversal of volumetric strain rate or peak stress).

In Figure 9, the engineering shear strain (axial strain minus lateral strain) increment is plotted against lithophysal porosity for 400 overburden, and peak-stress criterion. On the figure, the three lines (and similarly colored points) correspond to the three types of model (PFC circular voids, PFC irregular voids and UDEC circular voids). Finally, "error" bars for ±1 standard deviation are plotted in the same color as the corresponding line.

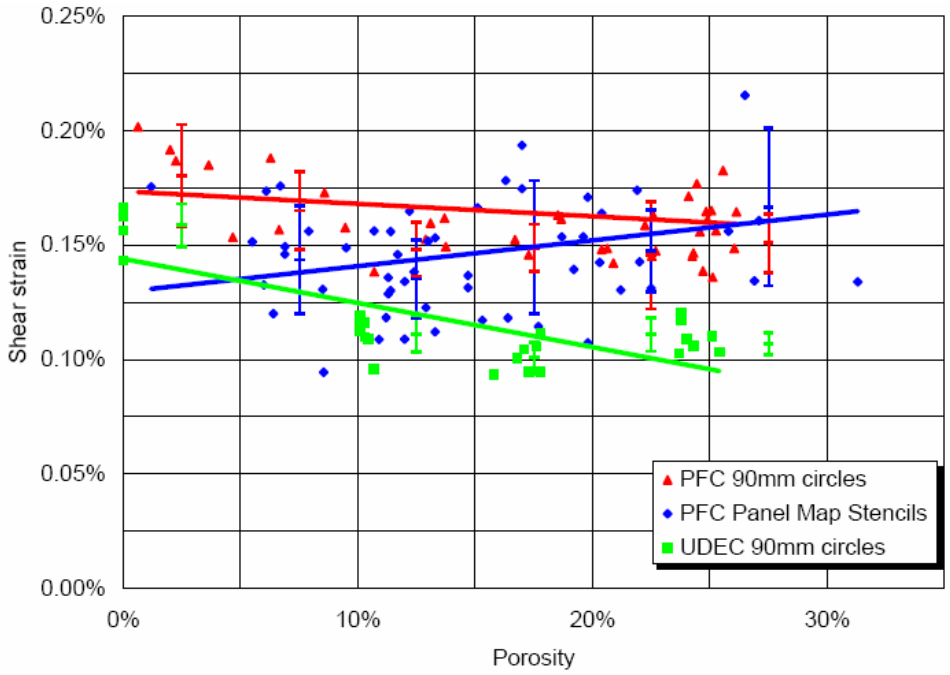

Figure 9 Shear strain vs porosity for peak-stress criterion; overburden = 400 m

2.5 Conclusions

Re-analysis of the laboratory results and the results of numerical simulations has provided a correlation between the mean shear strain experienced by a rock mass and the damage on internal structures (lithophysae). Because it appears that no damage (i.e., systematic cracks around and between lithophysae) is observed at the site, then the maximum shear strain over geological time is likely to have been between 0.1% and 0.2%. For the 288-mm diameter samples (shown in Figure 8), which are probably the best representation of the mechanical behavior of lithophysal rock, the majority of the results are in the range between 0.1% and 0.2% of strain.

3.0 REFERENCE

Itasca Consulting Group, Inc. (2004) *FLAC (Fast Lagrangian Analysis of Continua)*, Version 5.0 User's Manual. Minneapolis: ICG.